# REPORT DOCUMENTATION PAGE

Form Approved OMB NO. 0704-0188



| 1. REPORT DATE (DD-MM-YYYY) | 2. REPORT TYPE | 3. DATES COVERED (From - To) |
|---|---|---|
| 01-08-2017 | Final Report | 1-May-2013 - 30-Apr-2017 |

**4. TITLE AND SUBTITLE**
Final Report: Modulation Spectroscopy and Opto-Mechanics of Micro Toroidal Resonators

**5a. CONTRACT NUMBER**
W911NF-13-1-0140

**5b. GRANT NUMBER**

**5c. PROGRAM ELEMENT NUMBER**
206022

**6. AUTHORS**

**5d. PROJECT NUMBER**

**5e. TASK NUMBER**

**5f. WORK UNIT NUMBER**

**7. PERFORMING ORGANIZATION NAMES AND ADDRESSES**
University of Texas at Brownsville/Texas S(
One West University Blvd

Brownsville, TX 78520 -4933

**8. PERFORMING ORGANIZATION REPORT NUMBER**

**9. SPONSORING/MONITORING AGENCY NAME(S) AND ADDRESS (ES)**
U.S. Army Research Office
P.O. Box 12211
Research Triangle Park, NC 27709-2211

**10. SPONSOR/MONITOR'S ACRONYM(S)**
ARO

**11. SPONSOR/MONITOR'S REPORT NUMBER(S)**
62740-PH-REP.5

**12. DISTRIBUTION AVAILIBILITY STATEMENT**
Approved for public release; distribution is unlimited.

**13. SUPPLEMENTARY NOTES**
The views, opinions and/or findings contained in this report are those of the author(s) and should not contrued as an official Department of the Army position, policy or decision, unless so designated by other documentation.

**14. ABSTRACT**

**15. SUBJECT TERMS**

| 16. SECURITY CLASSIFICATION OF: | | | 17. LIMITATION OF ABSTRACT | 15. NUMBER OF PAGES | 19a. NAME OF RESPONSIBLE PERSON |
|---|---|---|---|---|---|
| a. REPORT | b. ABSTRACT | c. THIS PAGE | | | Malik Rakhmanov |
| UU | UU | UU | UU | | 19b. TELEPHONE NUMBER: 956-882-6746 |

# RPPR Final Report
as of 30-Oct-2017

Agency Code:

Proposal Number: 62740PHREP **Agreement Number: W911NF-13-1-0140**
**INVESTIGATOR(S):**


**Name:** Malik Rakhmanov
**Email:** malik.rakhmanov@gmail.com
**Phone Number:** 9568826746
**Principal:** Y

**Name:** Volker Quetschke
**Email:** Volker.Quetschke@utb.edu
**Phone Number:** 9568826723
**Principal:** N

Organization: **University of Texas at Brownsville/Texas Southmost College**
Address: One West University Blvd, Brownsville, TX 785204933
Country: USA

DUNS Number: 800187965 EIN: 742759269
**Report Date:** 31-Jul-2017 Date Received: 01-Aug-2017
**Final Report** for Period Beginning 01-May-2013 and Ending 30-Apr-2017
**Title:** Modulation Spectroscopy and Opto-Mechanics of Micro Toroidal Resonators
**Begin Performance Period:** 01-May-2013 **End Performance Period:** 30-Apr-2017
**Report Term:** 0-Other

Submitted By: Malik Rakhmanov Email: malik.rakhmanov@gmail.com
Phone: (956) 882-6746

**Distribution Statement:** 1-Approved for public release; distribution is unlimited.

**STEM Degrees:** 3 **STEM Participants:** 2

**Major Goals:** The main goal of this research is to transfer the techniques of phase-modulation spectroscopy developed for large-scale Fabry-Perot cavities to micro-ring resonators. For this purpose, we formed collaboration between UTRGV and Rice University. We planned 1) to acquire research instrumentation for experimental studies of micro-ring resonators on campus at UTRGV, 2) to initiate training of the UTRGV students in nano fabrication and clean room techniques, 3) to conduct experiments with silicon micro-ring resonators, and 4) to develop techniques for their characterization using the RF modulation spectroscopy.

**Accomplishments:** We have accomplished all major goals outlined in the initial proposal for this research. (For details see the uploaded Report). In particular,

1) We have acquired the knowledge of nanofabrication of Si microring resonators in Clean Room at the Nanofab Shared Facility of the University of Houston. After many trials and errors we successfully designed and fabricated our own Si-integrated devices and demonstrated that they work.

2) We development several experiments using the methods of modulation spectroscopy applied to optical cavities including the triangular ring resonators powered by Nd:YAG laser and the Si-integrated micro-ring resonators powered by tunable laser at 1550 nm and use the phase-modulation sidebands with frequencies up to 20 GHz.

3) We conducted a number of experiments with resonant sidebands and analyzed the data. The phase modulation spectroscopy allows us to deeply probe the structure of the resonance of the micro-ring resonators and understand their dynamics.

4) The results of these experiments show that the ideas initially proposed for this research are feasible and the data is promising.

# RPPR Final Report
as of 30-Oct-2017

**Training Opportunities:** During this reporting period PI and his students acquired training in nanofabrication techniques at the Nanofab Facility of the University of Houston. We learned practicing nano fabrication using E-Beam Lithography (EBL), Scanning Electron Microscope (SEM), and Reactive Ion-Etching (RIE) techniques.

The students involved in this project attended the IEEE Photonics Conference in Reston, VA, Oct. 4—8, 2015.

**Results Dissemination:** PI of this project was involved in outreach activity called “HIGH Scholars” which is a 9-week Summer Research Program organized by the University of Texas Rio Grande Valley and aimed at engaging local high-school students in research projects in STEM disciplines. The program became widely popular among the residents of South Texas and involved more than 100 students from local high schools. The PI served as a mentor for a high school student participating in a project which involved basic optics. The PI also gave tours of the lab to high-school students, their teachers and parents, and explained the significance of his research to the local community, emphasizing the importance of STEM education.

Other activities: PI presented an invited talk “Optical Heterodyne Techniques for Interferometric Measurements of Very Small Displacements and Phases” at the International Conference on Terahertz emission, Metamaterials and Nanophotonics TERAMETANANO-2016, April 3, 2016, Cartagena, Colombia.

A more extended version of this talk was presented by the PI at a Colloquium for Department of Physics, Embry-Riddle Aeronautical University, Prescott, AZ, on April 22, 2016

**Honors and Awards:** May 22, 2013
2013 SPIE Optics and Photonics Education Scholarship awarded to MS student Liliana Ruiz-Diaz for research in nano photonics under supervision of Dr. Rakhmanov.

February 11, 2016
Special Breakthrough Prize in Fundamental Physics for detection of gravitational waves. https://breakthroughprize.org/News/32

May 5, 2016
Award for Outstanding New Faculty Mentorship, University of Texas Rio Grande Valley, Edinburg, TX

January 4, 2017
2016 Gruber Cosmology Prize for participation in the discovery made by the LIGO Team.

**Protocol Activity Status:**

**Technology Transfer:** Patents Awarded during the reporting period:
Method and apparatus for modulating light US 8446657 B2

**PARTICIPANTS:**

**Participant Type:** Graduate Student (research assistant)
**Participant:** Anton Gribovskiy
**Person Months Worked:** 12.00 **Funding Support:**
Project Contribution:
International Collaboration:
International Travel:
National Academy Member: N
Other Collaborators:

**Participant Type:** Graduate Student (research assistant)
**Participant:** Artemiy Bogdanovskiy
**Person Months Worked:** 11.00 **Funding Support:**
Project Contribution:
International Collaboration:
International Travel:

National Academy Member: N
Other Collaborators:

**Participant Type:** Undergraduate Student
**Participant:** Guillermo Vazquez
**Person Months Worked:** 6.00 **Funding Support:**
Project Contribution:
International Collaboration:
International Travel:
National Academy Member: N
Other Collaborators:

**Participant Type:** Postdoctoral (scholar, fellow or other postdoctoral position)
**Participant:** Maxim Sumets
**Person Months Worked:** 8.00 **Funding Support:**
Project Contribution:
International Collaboration:
International Travel:
National Academy Member: N
Other Collaborators:

**Participant Type:** Undergraduate Student
**Participant:** Johnathan Aguillar
**Person Months Worked:** 4.00 **Funding Support:**
Project Contribution:
International Collaboration:
International Travel:
National Academy Member: N
Other Collaborators:

**Participant Type:** Graduate Student (research assistant)
**Participant:** Darkhan Tuyenbayev
**Person Months Worked:** 9.00 **Funding Support:**
Project Contribution:
International Collaboration:
International Travel:
National Academy Member: N
Other Collaborators:

**ARTICLES:**

# RPPR Final Report
as of 30-Oct-2017

**Publication Type:** Journal Article Peer Reviewed: Y **Publication Status:** 1-Published
**Journal:** Nano Letters
Publication Identifier Type: DOI Publication Identifier: dx.doi.org/10.1021/nl401591k
Volume: 13 Issue: First Page #: 3698
Date Submitted: 8/1/17 12:00AM Date Published: 7/29/13 5:21AM
Publication Location:
**Article Title:** Excitation and Active Control of Propagating Surface Plasmon Polaritons in Graphene
**Authors:** Weilu Gao, Gang Shi, Zehua Jin, Jie Shu, Qi Zhang, Robert Vajtai, Pulickel M. Ajayan, Junichiro Kono, a
**Keywords:** Active plasmonics, graphene surface plasmon polaritons, infrared optoelectronics, nanophotonics
**Abstract:** We demonstrate the excitation and gate control of highly confined surface plasmon polaritons propagating through monolayer graphene using a silicon diffractive grating. The normal-incidence infrared transmission spectra exhibit pronounced dips due to guided-wave resonances, whose frequencies can be tuned over a range of ?80 cm?1 by applying a gate voltage. This novel structure provides a way to excite and actively control plasmonic waves in graphene and is thus an important building block of graphene plasmonic systems.

Acknowledged Federal Support: **Y**

31 July, 2017

Contract: W911NF-13-1-0140
Title: Modulation Spectroscopy and Opto-mechanics of Micro Toroidal Resonators
PI: Malik Rakhmanov

University of Texas Rio Grande Valley
1 West University Blvd.
Brownsville, TX 78520

# Final Report
## for period beginning May 1, 2013 and ending April 30, 2017

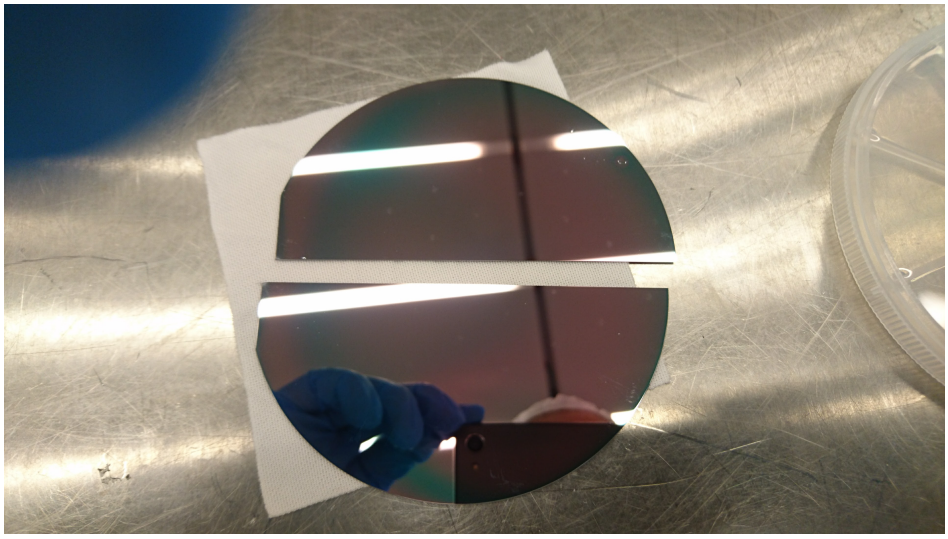

## Table of Contents

## Introduction

Frequency and phase modulation sidebands play an important role in cavity locking and laser frequency stabilization [1] and [2]. They can be used for precision measurement of various cavity parameters including FWHM of resonance, g-factor, mirror curvature [3], etc. Further development of the modulation techniques is presented in a recent paper "High precision optical cavity length and width measurements using double modulation" [4] co-authored by PI and which is based on a technique previously developed by the PI and his collaborators. (The present award is acknowledged in this paper.) The main idea of this paper is to apply phase modulation sidebands 1-FSR away from the carrier. This method was successful for large cavities with the length of several meters. It will be difficult to apply this method to micro resonators as it would require a very high modulation frequency (e.g. 100 GHz or 1 THz).

Instead, here we consider to have the modulation sidebands resonating on the same FSR peak with the carrier. This is the idea behind the experiments proposed within the present project. We have modified the method accordingly and designed the following layout (Fig. 1). We first complete a pilot experiment with the Nd:YAG laser locked on a mid-size resonator which is a triangular 3-mirror cavity built with a fused silica spacer. The corresponding modulation frequency varies from a few kHz to 200 MHz.

## Pilot Experiment with a Tunable Triangular Resonator (2015)

### Schematic Diagram of the Experiment

Based on the schematic from Fig. 1 an optical layout was built at UTRGV by the PI and his students. The photo of the experiment is shown in Fig. 2. The resonator made of fused silica (white object near the center of the picture) was built previously by one of the UTRGV students working under the supervision of the PI. Nd:YAG laser with output power 500 mW is in the upper left corner of the picture. Since the laser is not tunable the cavity has a PZT actuator for control of its length.

There are two EOMs in this experiment: one for locking the cavity (EOM1) using the reflected beam and another (EOM2) for providing the modulation sidebands in the transmitted beam. The PDH signals are obtained from two photo-detectors with two crossed polarizers to separate S and P polarizations of the reflected laser beam (PD1 and PD2). The In-phase (I) and Quadrature (Q) signals produced by the modulation sidebands resonating in the cavity are measured with SRS 200-MHz lock-in amplifier (LAMP).

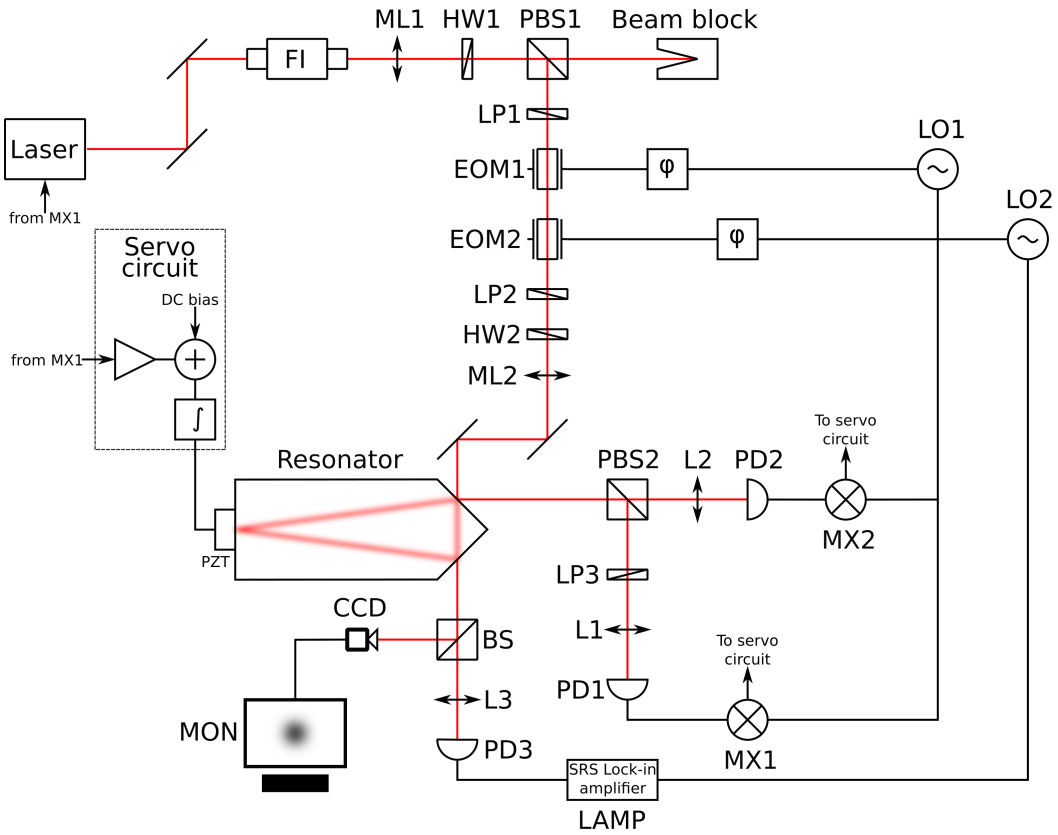


Figure 1. Schematic layout of the experiment with Nd:YAG laser and a tunable triangular ring resonator.

Locking of the cavity to the laser is done with a servo electronics built by the students for this experiment. After beam alignment, modematching, and cavity locking the experiments with resonant sidebands began. Selected results of these experiments are shown on the next page.

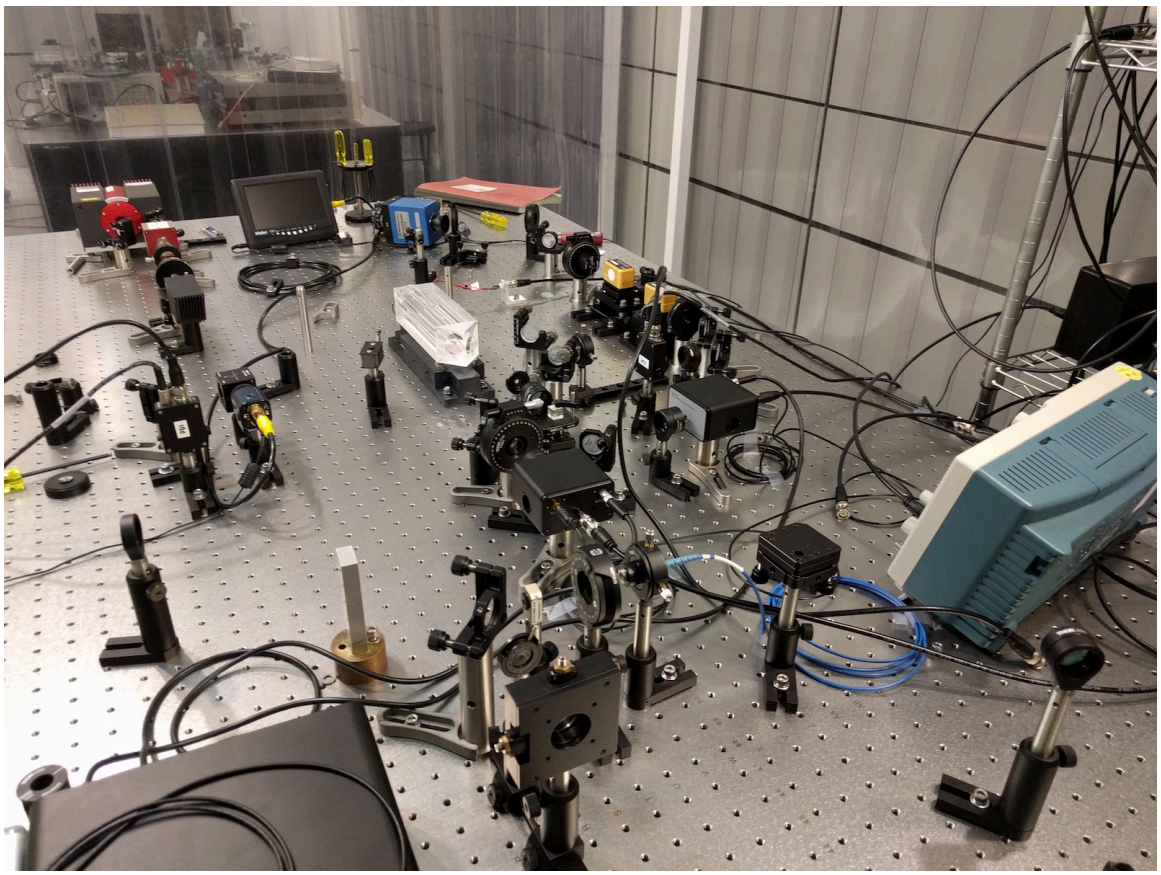

Figure 2 Table-top setup with Nd:YAG laser and the tunable triangular resonator (a white rectangular object near the center of the optical table.)

## Measurement Results

We conducted the following experiment: the light from the laser was phase-modulated (EOM-1) to produce the Pound-Drever-Hall signal [1] in reflection. This signal was used to lock the cavity to the carrier frequency with the servo electronics controlling one of the cavity mirrors through the PZT. The modulation sidebands (EOM-2) are forced to resonate in the cavity on the same peak occupied by the carrier. They are detected by the photodiode in transmission.

Next, a small (less than HWHM) offset was introduced to the servo to shift the carrier from the center of the resonance. The offset locking allowed two signals emerge from I and Q demodulation outputs of the modulated intensity at the photodiodes. They are shown in Fig. 3. (Here I and Q signals are denoted by X and Y.) As was shown in paper by Staley et al. [4], the zero crossing of the Q signal yields an accurate measurement of the cavity width (HWHM).

Based on the results of the pilot experiment we were able to design and build an experiment for testing the micro-ring resonators embedded in silicon integrated photonic circuit. This experiment is described next.

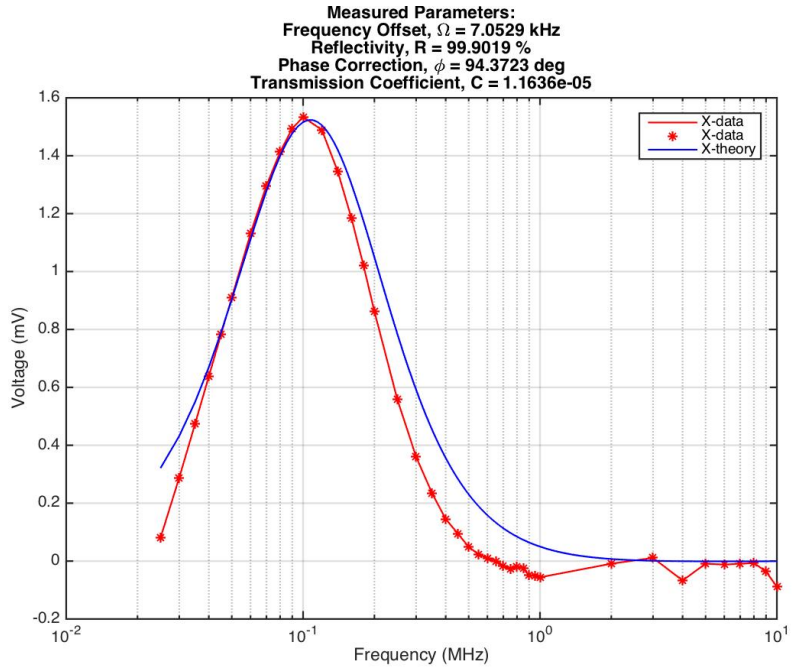


Figure 3. In-phase (I) demodulated signal. Comparison of the theory and experiment.

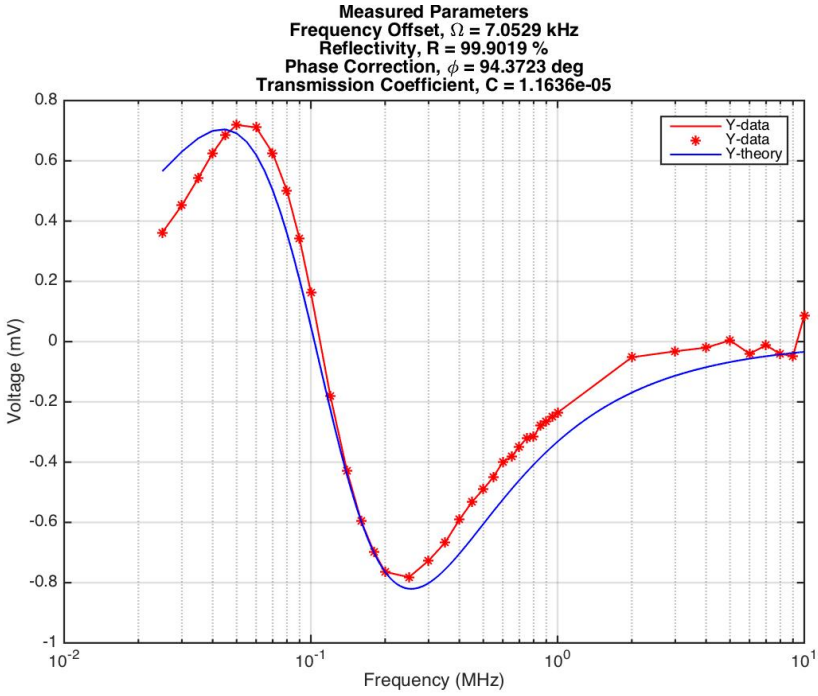


Figure 4. Quadrature (Q) demodulated signal. Comparison of the theory and experiment.

## Design and Fabrication of Microring Resonators

We had wafers with crystalline Si device layer and more recently we obtained wafers with amorphous Si device layer. Thus, for experiments in the lab we had both wafers with crystalline silicon and wafers with amorphous silicon.

We designed all our devices using KLayout. Our current design has a U-shaped waveguide to deliver light to microring resonators. We designed several configurations: microrings with 100, 60 and 5 micron diameter shown below. To make coupling coefficients the same for different sizes of the microrings we keep constant curvature of the waveguide in the proximity of the resonator.

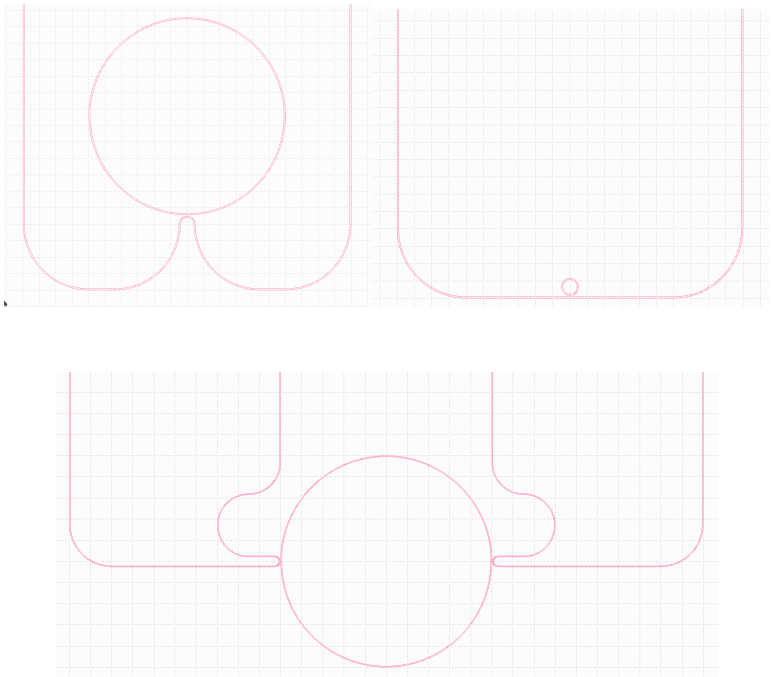

Figure 5. Various trial design configurations for waveguide-microring devices on the SOI wafer for fabrication.

### Design Considerations

We tried to extend waveguides by adding tapers to improve the coupling efficiency between free space laser light and waveguide. The waveguides have a standard width of 450 nm. This width expands to 20 micron at the end of the taper. The improvement in the coupling was not significant. However, this design drastically increased E-beam printing time. Therefore, we abandoned this scheme.

### Fabrication based on PMMA (2015)

We fabricated devices using our double mask procedure which consists of the following steps:

- Apply PMMA positive photoresist to the sample
- Write patterns with E-beam (photoresist exposed to E-beam will be removed)
- Develop the sample
- Cover the sample with chromium
- Lift rest of PMMA with chromium in acetone
- Define waveguides with reactive ion etching.

(Chromium prevents silicon from been etched.)

We also optimized the etching process. Our recipe for RIE consists of the following parameters:

| | | |
|---|---|---|
| RF power | W | 70 |
| ICP power | W | 1500 |
| Pressure | mtorr | 6 |
| Argon | sccm | 40 |
| CHF3 | sccm | 10 |
| Temperature | C | 20 |

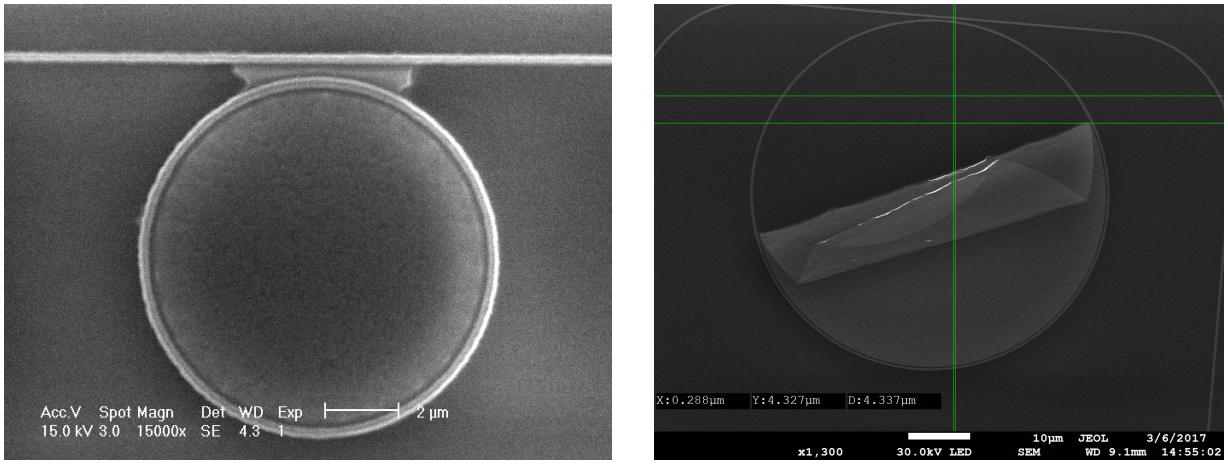


Figure 6. Examples of fabrication errors in the process based on chromium mask: incomplete or partial removal of the chromium mask.

The main problem with this process is the lift-off step. Chromium can remain in the area inside of the ring (Figure 6 left) or sometimes it is not completely removed (Figure 6 right). To fix the problem we increase the duration of the lift-off step while the sample is submerged in acetone. However, long exposure of the sample to acetone makes the edges of the chromium mask too rough causing the waveguides to become thinner than designed, eventually damaging them.

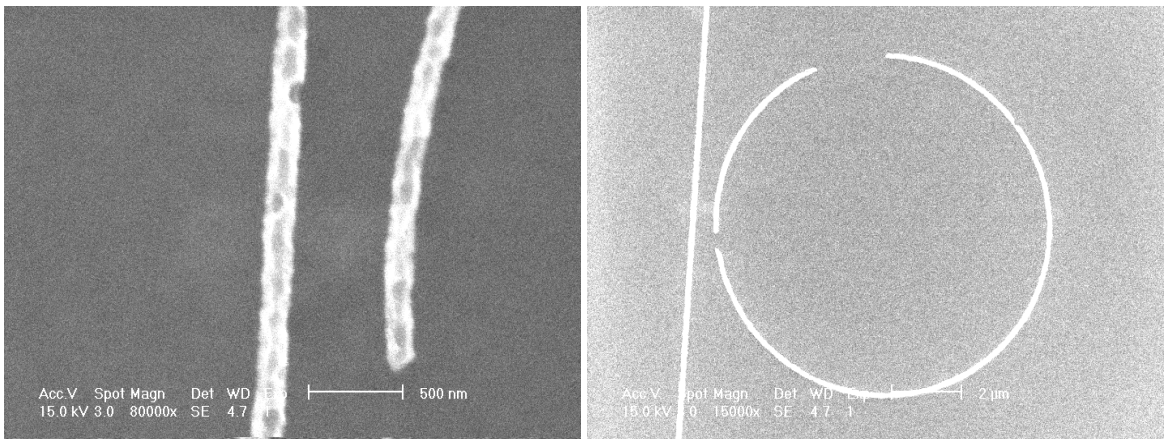

Figure 7. Examples of fabrication errors in the process based on chromium mask: overexposure of the sample to acetone.

To improve the lift-off process we used two layers of PMMA: bottom layer has smaller molecular weight than the top one, which creates an undercut after E-beam exposure and helps during the lift-off. Also we optimized the time of exposure to acetone in the ultrasonic bath.

**Fabrication based on HSQ (2016)**

To improve the fabrication process we decided to get rid of the chromium step. For this we had to switch to negative photoresist: HSQ (XR-1541). After exposure to E-beam and development stage the negative photoresist stays at exposed areas. This allows us to simplify the fabrication process and get rid of the steps with Cr deposition and its subsequent liftoff. The new process consists of the following steps:

- Apply HSQ photoresist to the sample
- Expose the sample to E-beam
- Develop the sample
- Define waveguides with reactive ion etching

In this case the etching recipe is different from the one we used to etch silicon with chromium mask.

By numerous trials we found that the following recipe gives best results:
http://www.pythography.com/processes/rie/rie.html (recommended by the UH Nanofab staff)

| | | |
|---|---|---|
| RF power | W | 30 |
| ICP power | W | 450 |
| Pressure | mtorr | 10 |
| SF6 | sccm | 30 |
| C4F8 | sccm | 45 |
| O2 | sccm | 3 |
| Temperature | C | 20 |

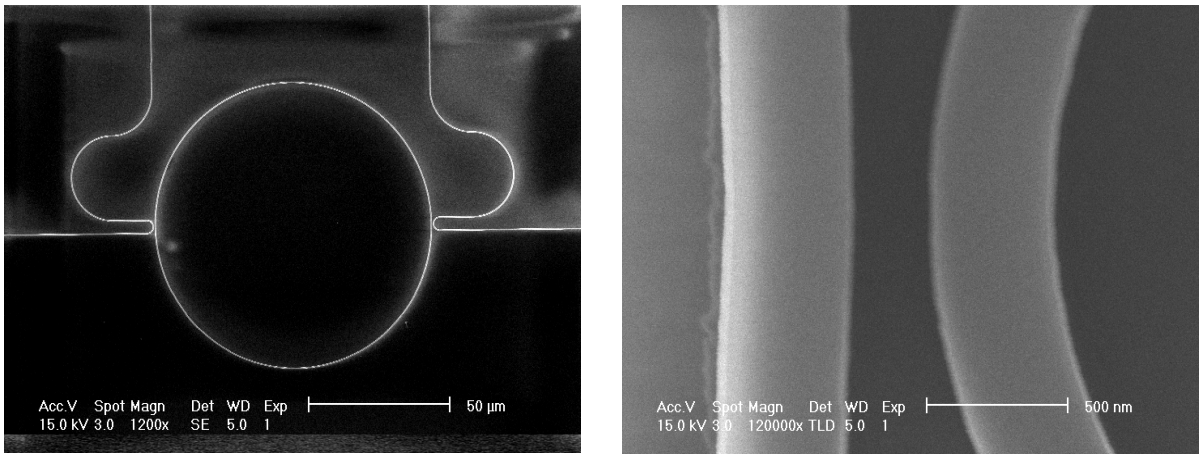

Figure 8. Successful fabrication of the microring resonator with two waveguides for light coupling.

Figure 8 shows the SEM scan of the device fabricated with the HSQ Process. Left: Microring resonators with two waveguides corresponding to ``add" and ``drop" channels. They look like ``ears" due to their curved shaped. This geometry was picked intentionally so that we can control the evanescent coupling of light from the waveguide to the microring. Right: zoomed view of the area where the drop channel comes close to the microring. Note that the waveguide is not touching the resonator. There is a finite gap. The light couples by evanescent field. The SEM scan (right) shows that the gap between the waveguide and the resonator is 300 nm as was designed. As can been seen significant improvement was made to the quality of the device: the walls of the waveguides and microring are smooth and there are no visible imperfections.

## Cleaving of Wafer Devices

In the beginning we were cutting our Si samples with a dicing saw. The results were not satisfactory. Almost always we ended with rough edges of the sample. Later we switched to cleaving using the natural tendency of the sample to break along the crystallographic planes of Si.

We couple light into waveguides from the butt-end. For this we have to cleave our samples which can have a somewhat unpredictable result. To increase the probability of successful cleaving we extended the waveguides by 500 µm and placed the devices in groups (Fig. 9). When the cleaving line runs horizontally across the sample, i.e. along the

horizontal rule lines, it will cut through one of the devices properly. This arrangement is done in such a way that in any outcome there will be at least one of cleaving line that cuts the device in the appropriate region. This idea proved to be successful.

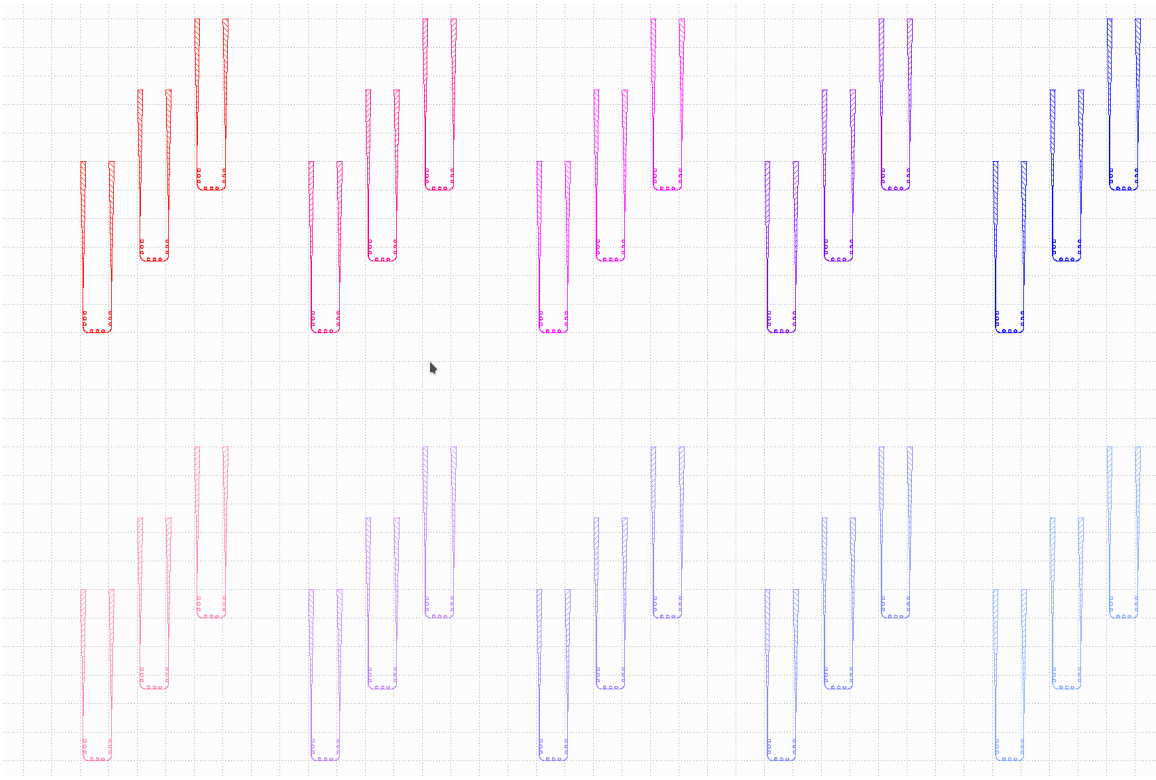

Figure 9. Custom design of the Si devices and their placement on the sample. Note the staircase arrangement of the group of the devices optimized for cleaving.

We have applied this idea in one of the fabrication trials. The resulting sample was then studied both with optical microscopy and SEM. As can be seen in Figure 10 (left), the cleaving edge is smooth and straight and the zoomed view (right) shows almost perfect vertical cut.

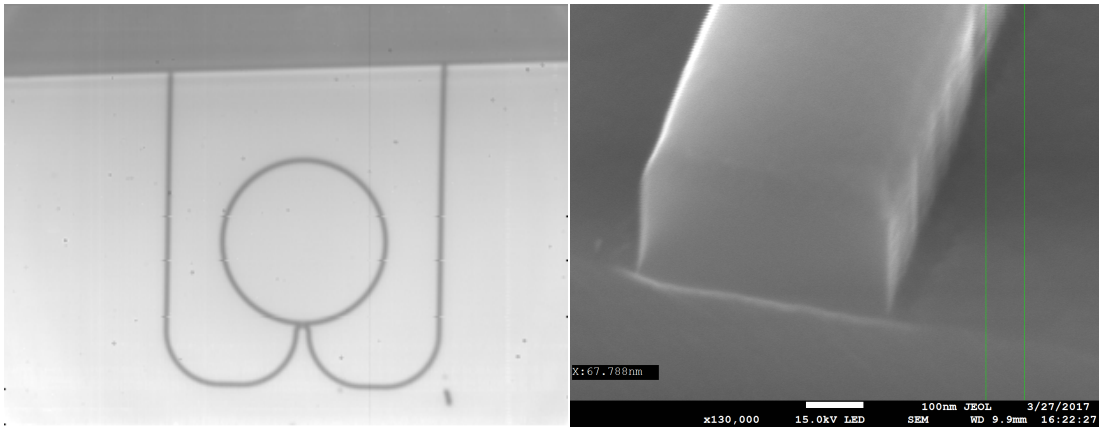


Figure 10. Successful results of cleaving. Left: optical microscope image (taken with SWIR camera in the lab) of one of the devices cleaved just at the right place. Right: SEM scan of the cleaved edge.

Note that this waveguide does not have tapered end. We fabricated devices with both tapered and non-tapered ends and found that there is no significant difference in coupling of the light.

## Experiments with Micro Toroidal Resonators

The layout for the experiment with micro resonators is shown in Fig. 11. It requires much higher modulation frequency (tens of GHz) than the experiment in Fig. 1. Over the last two years we conducted a number of experiments some of them using light in transmission (for amorphous Si) and others with the light in reflection (for crystalline Si).

### Schematic Diagram of the Experiment

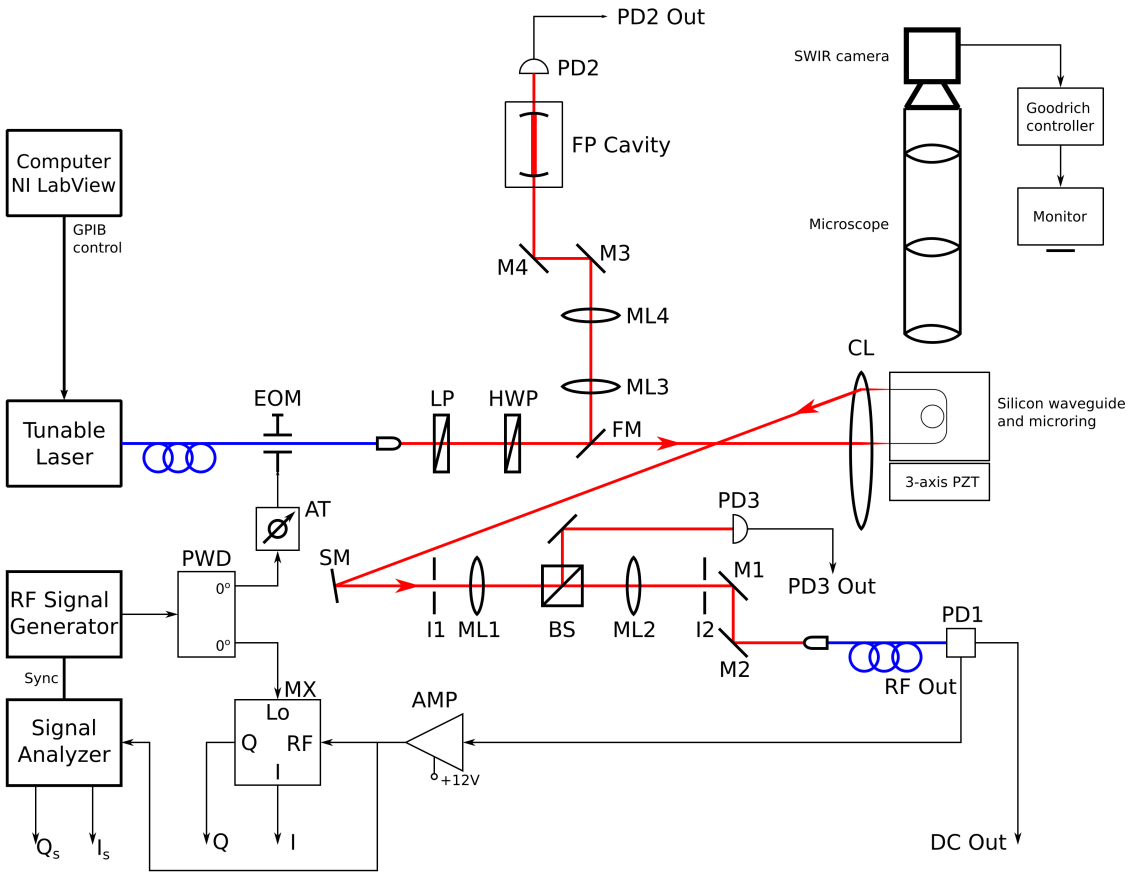


Figure 11. Schematic diagram of the experiment with silicon integrated optical circuit containing waveguides and micro-ring resonators. (Blue – optical fibers, red – free space laser beam.)

The experimental setup consists of a tunable laser (1480—1620 nm) which provides the light to the waveguide in the Si integrated photonic device. The laser beam is conditioned by mode-matching lenses and a micro lens (CL). The same lens is used for extracting light from the Si photonic device, which is fixed on a 3-axis PZT stage for precision alignment. The return light is mode-matched to couple to the fiber input of the fast RF photodiode (PD1). The output of the photodiode is amplified by the RF amplified (AMP) and is rectified by the mixer (MX). By tuning the laser frequency we can achieve resonance of light in individual micro-ring resonators in the device.

The RF Signal Generator provides the reference signal for both fiber-coupled EOM and the mixer (MX). A photo of the setup is shown in Figures 12 and 13.

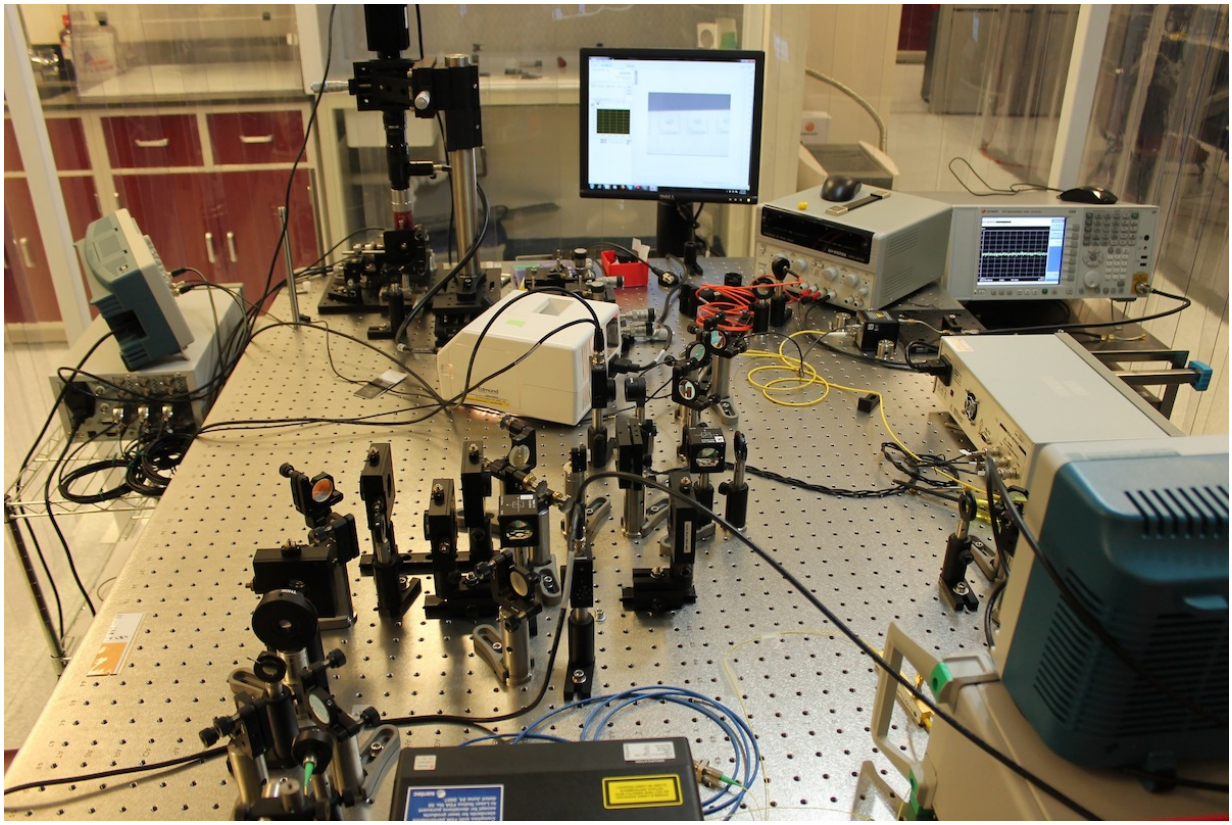

Figure 12. The front side of the experimental layout showing part of the laser and the beam conditioning optics, as well as photo detection part. The output of the SWIR camera is shown on the monitor displaying magnified view of the silicon nanophotonic device.

Table-top setup with silicon integrated photonic circuit. The micro-ring resonators are placed on the 3-axis PZT controller under the SWIR microscope. The monitor shows one of the waveguides brightly lit by the input light and the silicon micro-rings resonating the light at 1550 nm.

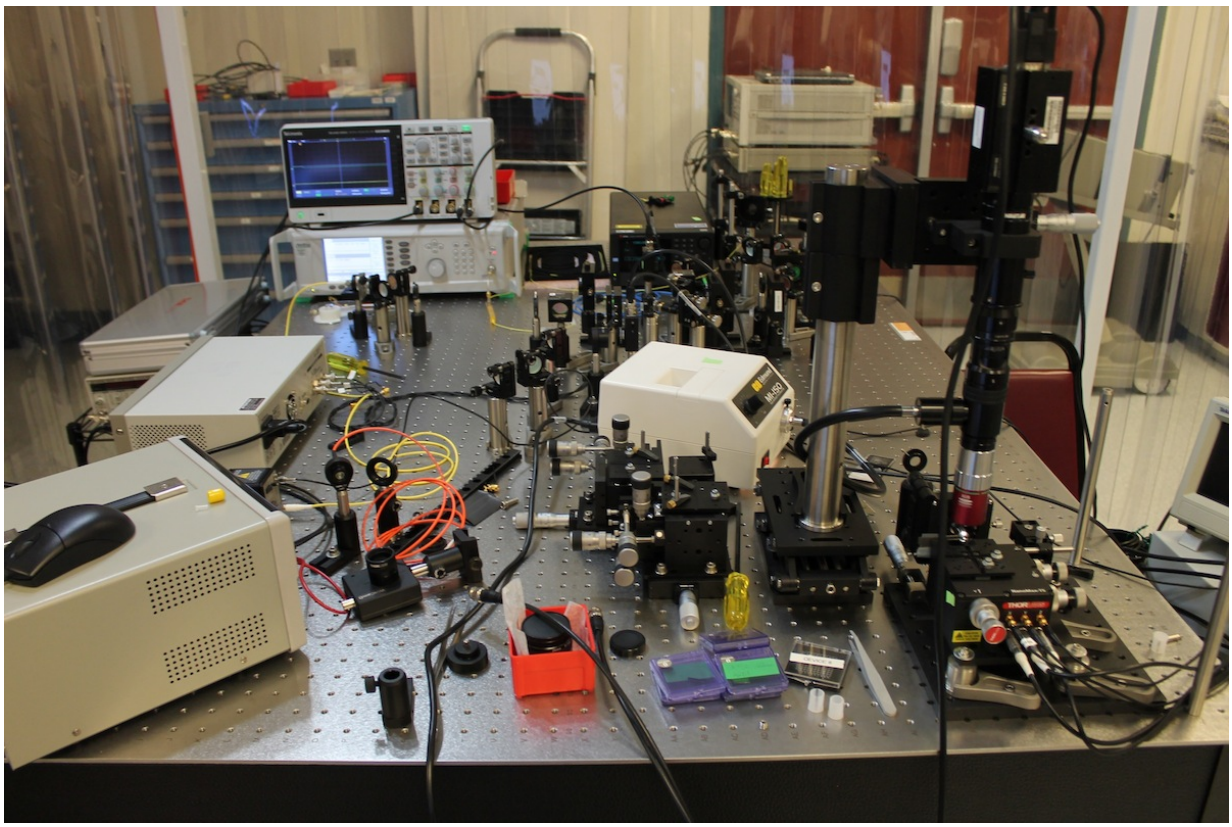

Figure 13. The back side of the experimental layout showing 3-axis PZT translational stage with silicon nanophotonic device positioned under SWIR microscope. The translational stage operates in the closed-loop regime to suppress noise due to mechanical vibrations.

## Experiments with Light in Transmission (Linear Regime)

With the table-top experimental layout in the lab at UTRGV we modematch the light from the tunable laser to a sample on the XYZ-positioning stage and align it for maximum coupling to one of the devices.

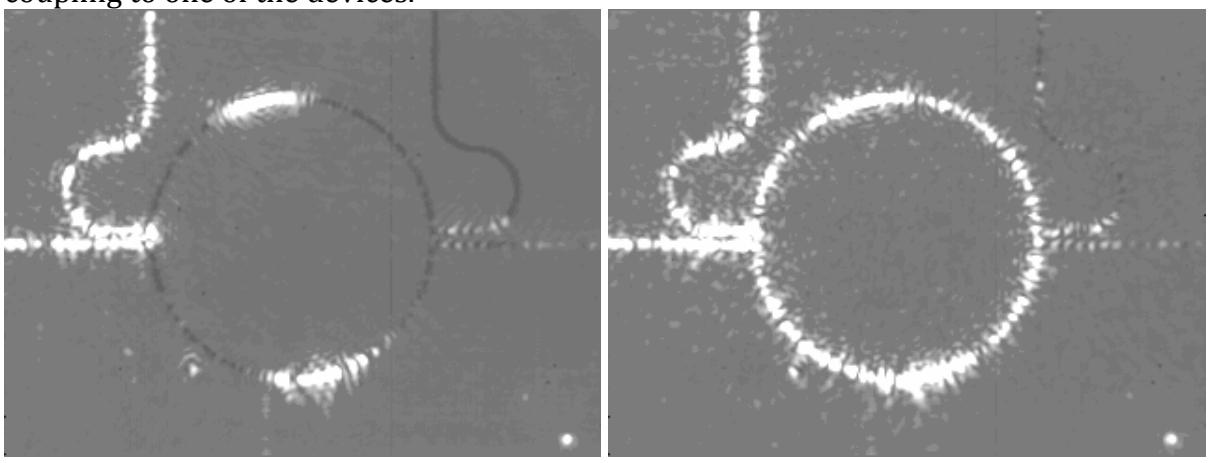

Figure 14. Successful coupling of light to one of the microring resonators that we fabricated (diameter: 200 micron, cross-section: 450x220 nm)

Figure 14 shows how one of the microrings comes to resonance. Left: an image taken with optical microscope image (with SWIR camera in the lab) of a micro-ring resonator with two waveguides: ``add" channel on the left side and ``drop" channel on the right side. Right: The same micro-ring resonator but with light tuned to resonate in it.

Note that the add channel is lit up in both left and right figures due to the light traveling along it. The micro-ring resonator is off resonance. The two bright spots on top and bottom are due to scattered light impinging on it from above.

## Measurement of FWHM in Transmission

In the experiment we scan the wavelength of light which is coupled to resonator (amorphous Si) via ``add" channel to achieve resonance. During the resonance the light builds up in the micro-ring and then tunnels to ``drop" channel. Using this channel we measure the full width at half maximum (FWHM) of the resonances.

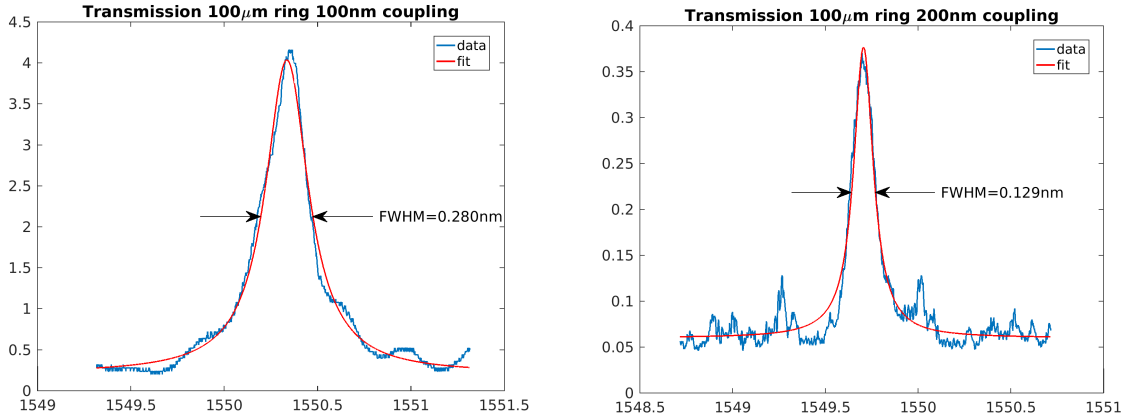


Figure 15. Measurement of the width of the resonance for two microring resonators: 100 nm gap (left) and 200 nm gap (right).

Left figure: the resonance of light in micro-ring device with 100 nm gap between the waveguide and the ring. Right figure: the resonance of light in micro-ring device with 200 nm gap between the waveguide and the ring. This way we control the coupling efficiency between the waveguide and the microring and thus change the quality factor of the resonances.

## Measurement of Results (2016)

Below we show two sets of measurements that were conducted in 2016. The first measurement involves scans of the laser frequency across one resonance of the micro-ring resonator. The second measurement involves scans of the modulation frequency for fixed frequency of the laser.

Figure 16 shows one of the many results of the first experiment. As we scan the laser frequency the light resonates in a particular micro-ring resonator which results in a dip of the intensity of the DC output on the photodiode (top plot). Note the abrupt switching of the resonance characteristic of the non-linear behavior of the silicon. Due to hysteresis of

this switching the scans forward and backward differ significantly. The modulation frequency was set to 9 GHz in this measurement.

In Figure 16 the scan forward is marked by (->) and scan backward is marked by (<-). The corresponding In-phase (I) and Quadrature (Q) demodulation signals are shown in bottom plot of Figure 16.

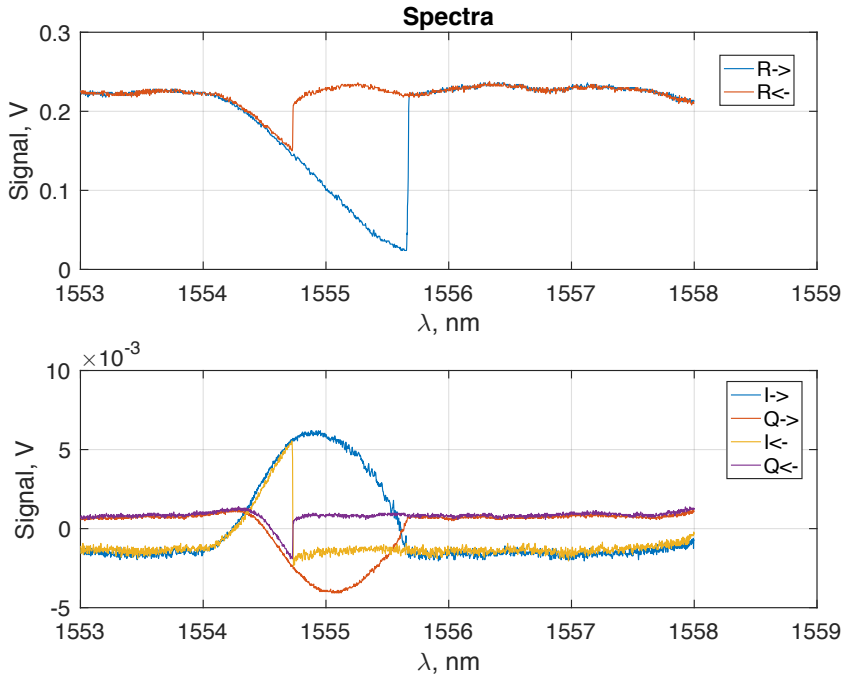


Figure 16: The response of a micro-ring resonator to the modulated laser field. Modulation frequency is set at 9 GHz. Top: the intensity of the reflected light in the waveguide with the characteristic Si nonlinear switching (blue – scan forward, red – scan backward). Bottom: I and Q demodulation outputs of the RF photodiode PD1 after the mixer.

The measurement in Figure 16 required significant data analysis to suppress the noise due to various imperfections including the RF pickup and crosstalk. In addition, background subtraction was implement to reduce some of the cross-talk.

Finally, we fixed the laser frequency near the peak of the resonance of one of the micro rings and slowly changed the modulation frequency. This second measurement is much harder than the first. In this case it is very hard to remove the noise due to RF pickup and crosstalk. However, we were able to complete the measurement. The results are shown in Figure 17. The range of the modulation frequency (from 3 GHz to 18 GHz) was set by the limitation of our mixer.

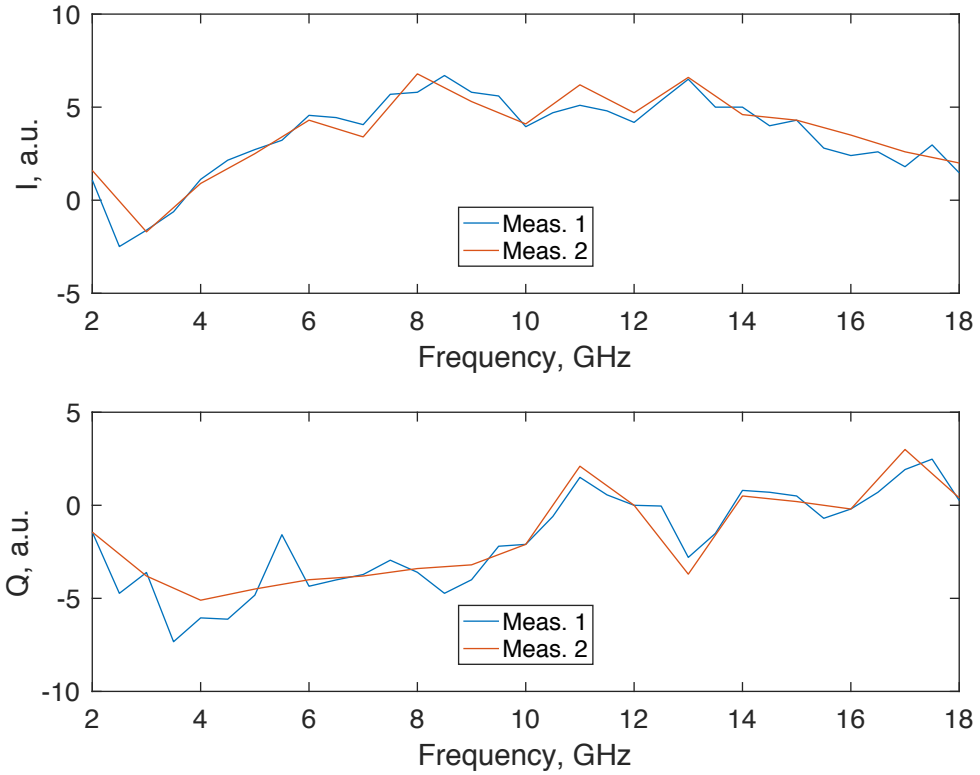


Figure 17: The dependence of I (top) and Q (bottom) signals on the modulation frequency.

The dependence of the demodulation signals on the modulation frequency as it varies from 2 to 18 GHz is shown in Figure 17. The I (top) and Q (bottom) signals were recorded for two independent measurements. This was the preliminary result (2016). It shows large variations of the signals due to systematic errors. Better measurement results were obtained in 2017 (see below).

## Experiments with Light in Reflection

### Measurement of the Reflected Spectra (2017)

The basic characterization of the microring resonator consists of a measurement of its power spectrum. In this measurement we detect the light reflected by the resonator and vary the wavelength of the incident laser beam. Figure 18 shows the spectrum of one of our crystalline Si microring resonators. In this figure we combined several measurements which correspond to different levels of the incident laser power as it varies from -5 dBm to +4 dBm as recorded on the laser control panel.

For convenience we present the normalized power spectrum (power set to 1 at max). As the power of the incident light increases the nonlinear effects begin to become more and more prominent: resonance shape is not symmetrical anymore (-2 dBm), and a sharp switching occurs between the resonating and non-resonating states at 1 dBm and 4 dBm.

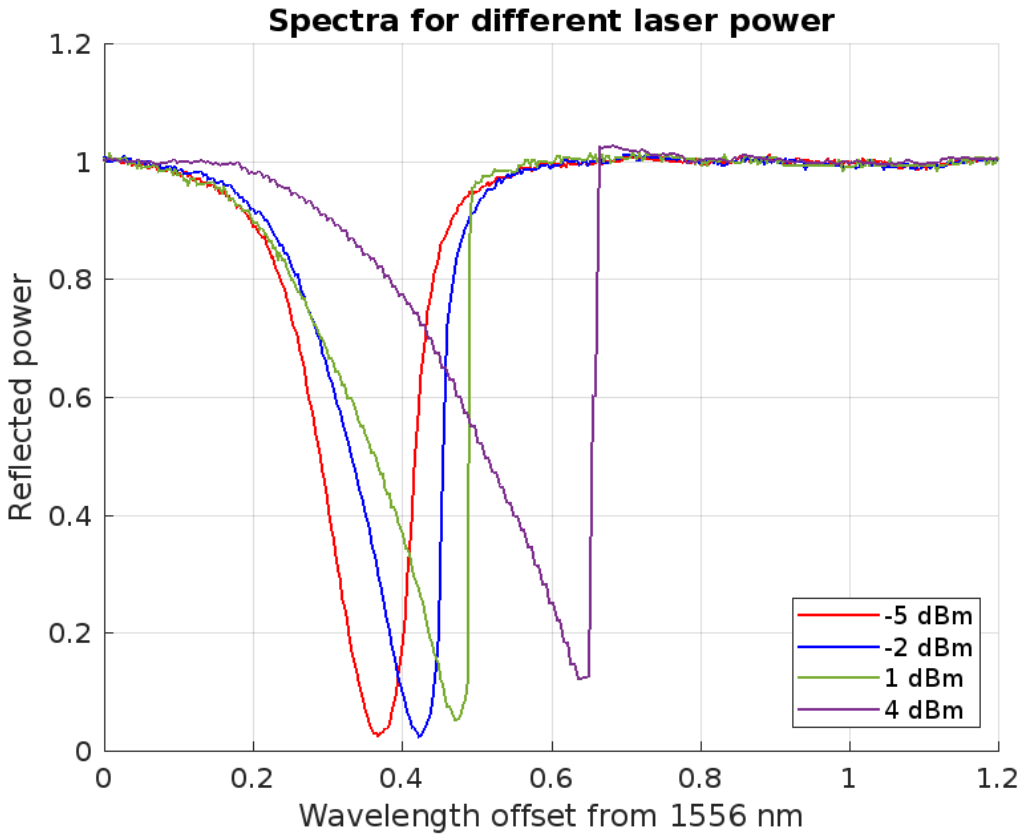


Figure 18. The spectrum of the reflected light intensity of one of the microring resonators.

## Measurement of I and Q Demodulation Outputs

The next set of measurements that we planned for this experiments is based on the resonant sidebands and synchronous demodulation of the modulated intensity of light reflected by the microring resonator.

In this experiment we scan the laser wavelength and measure the intensity (R) of light reflected from the ring (black trace) and the corresponding I and Q demodulation outputs. The idea for this experiment is taken from the pilot measurement that uses the mid-size triangular ring resonator described above. To put the graph on the same scale the data were multiplied by the scale factors for I and Q signals (max – min) on corresponding plots. Also it was shifted up in such of way that the zero on the R graph corresponds to maximum value of the I-Q signals.

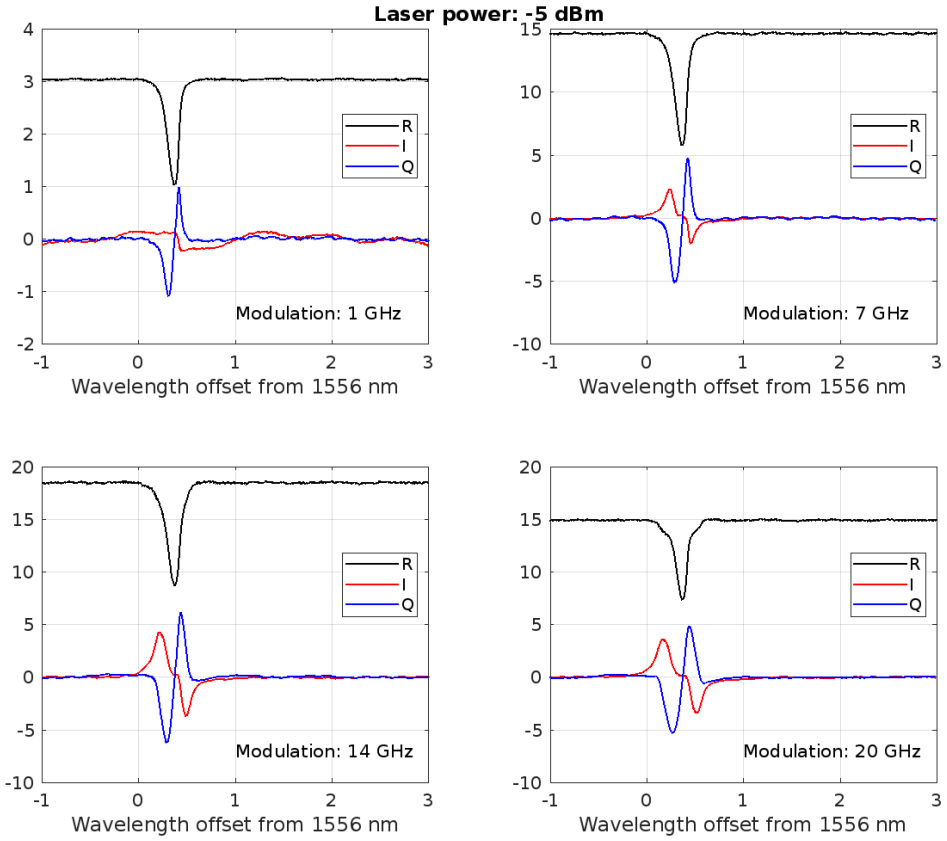


Figure 19. Combined measurement of R and I and Q signals in the linear regime (laser power is set to -5 dBm).

Figure 19 shows the response of the microring resonator in linear regime. The I and Q graphs are symmetric with respect to the center of the resonance. When we increase the frequency of modulation one can see that the sidebands start to appear on either side of the resonance peak. The peaks on I and Q graphs are also moving away with sidebands.

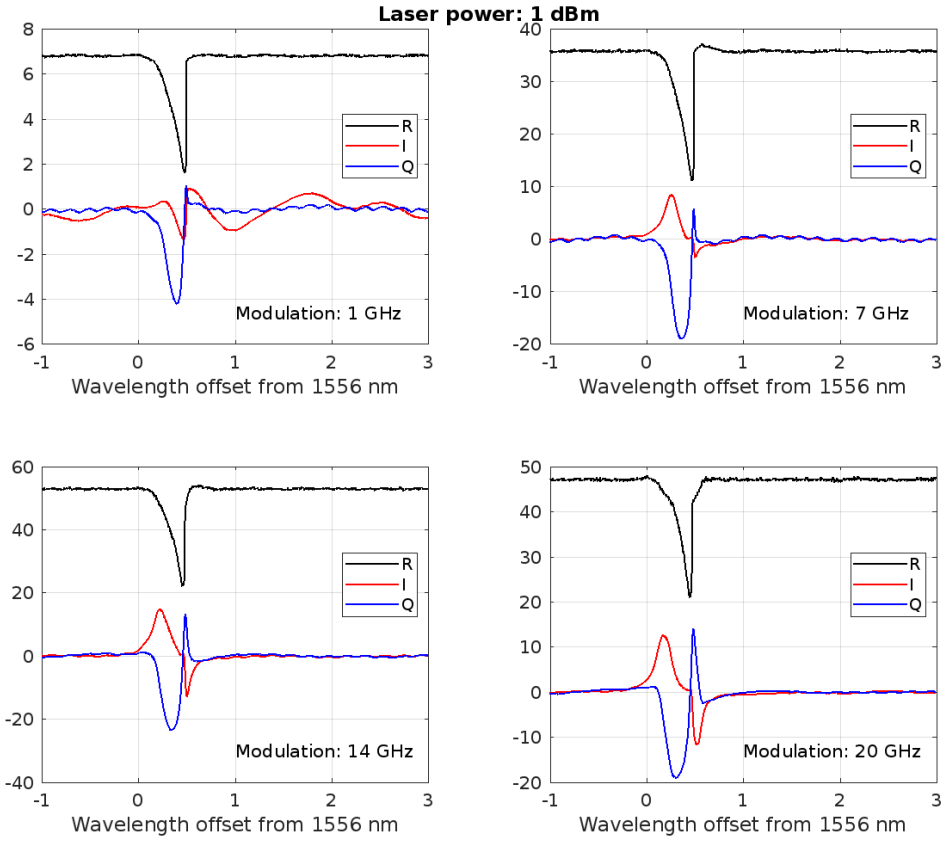


Figure 20. Combined measurement of R and I and Q signals in the weak non-linear regime (laser power is set to -1 dBm).

One can clearly see nonlinear effects start to emerge after increasing the laser power 4 times. Right after passing the resonance point the reflected power sharply increase. Despite this it is still possible to perform locking on the resonance, because the Q graph passes through zero which is why it is possible to use it as an error signal for a feedback circuit.

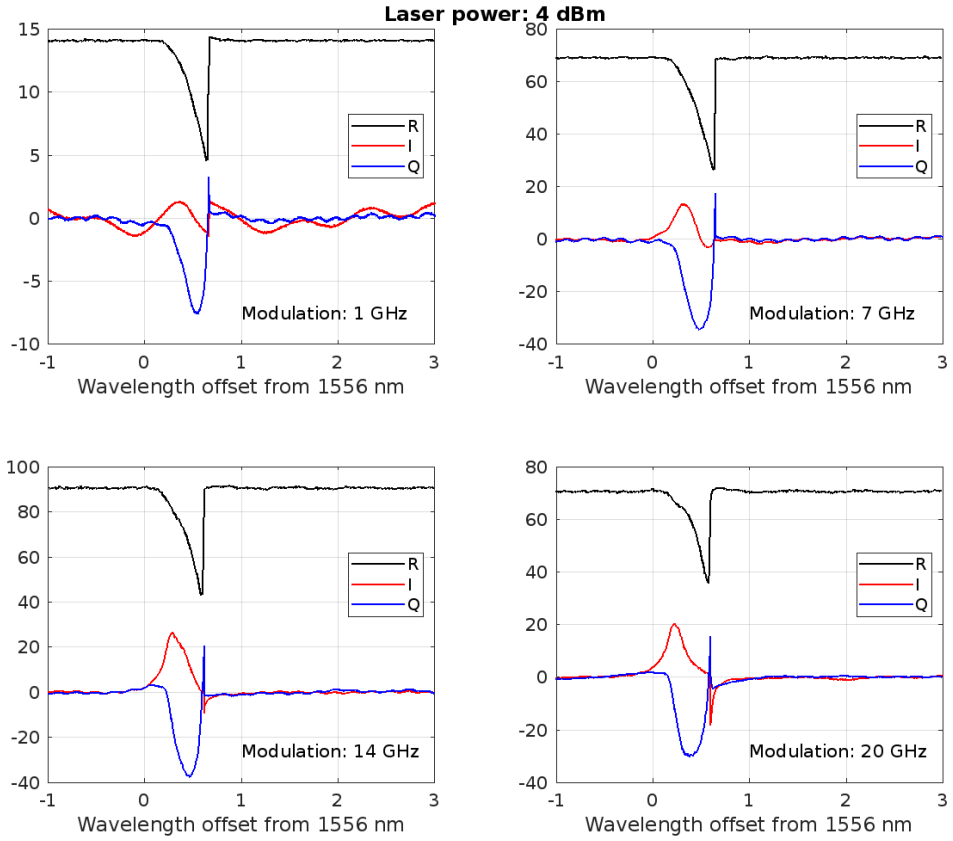


Figure 21. Combined measurement of R and I and Q signals in the strong nonlinear regime (laser power is set to 4 dBm).

After increasing the laser power by a factor of two the nonlinear switching is prominent and also the resonance wavelength increases. According to the Q graph switching still happens right after cavity reaches the resonance. These graphs are similar to the ones for 1 dBm input power, but resonance curve widens.

## Phasor Representation of the I and Q Signals

The previous measurements can be conveniently arranged in terms phasor diagrams. A phasor diagram shows the data in terms vector with components (I, Q) or (Q, I). The advantage of this representation is the clear phase dependence of the recorded signal.

Theoretically, the I and Q signals have a well defined phase. Therefore, their phasor diagram yield direct phase dependence as the modulation frequency varies within its range. This was essentially the mechanism behind the measurements reported in [1]. However, in practice a random phase enters the measurement due to imperfections and RF pickups.

First we measure the I and Q signals directly, i.e. without any post processing. In Figure 22, every graph represents a different trial, during which the laser wavelength is scanned

through the resonance. All parameters are left the same. These data are taken for -5 dBm laser power and modulation frequency of 20 GHz. Without the post processing, the I-Q phasors undergo random rotation from one measurement to another.

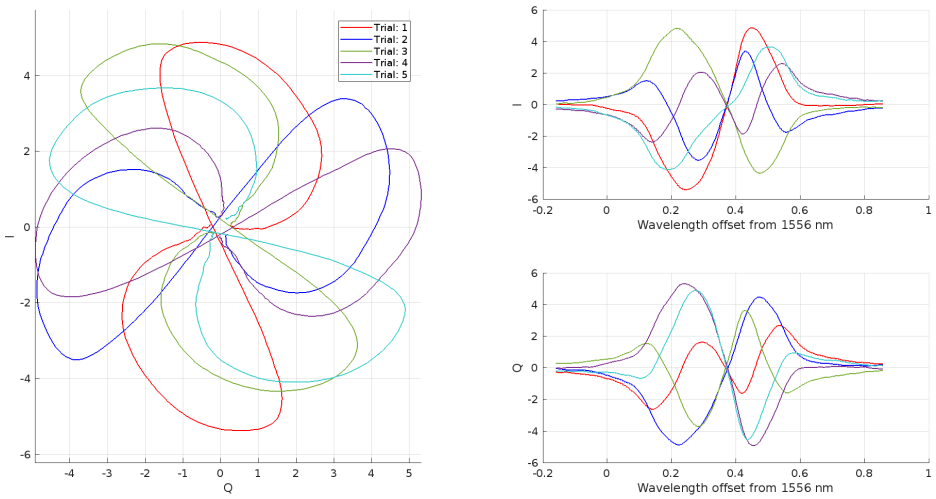


Figure 22. Unprocessed phase diagrams of the I-Q demodulation signals. Note the random change in their phase from one measurement to another.

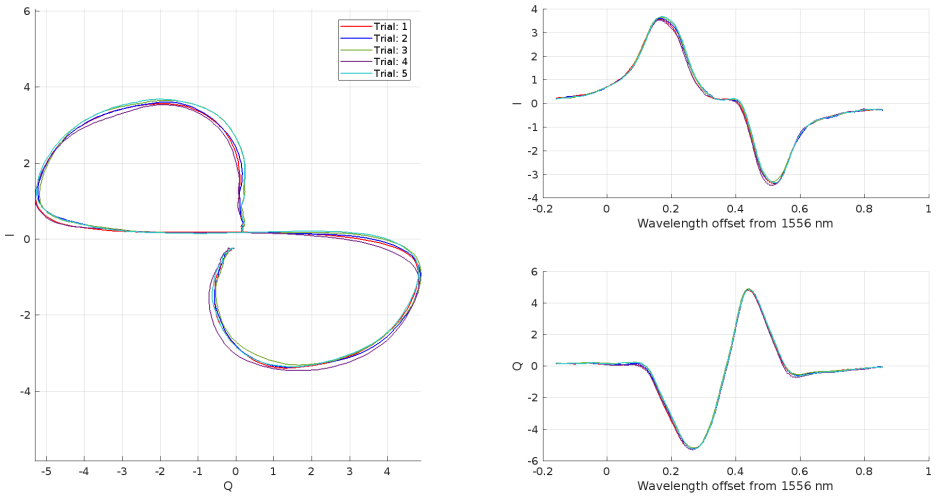


**Figure 23. The phase diagrams of the I-Q demodulation signals after they were adjusted for the same phase at the starting point. Note close alignment of all the traces.**

To get rid of such uncertainty we rotate data in such way that when laser wavelength passes through a resonance we minimize the change in I demod channel. In this case in the vicinity of the resonant point the I-signal has a cubic dependence on the wavelength offset, whereas the Q-signal has the linear dependence. Consequently the I-Q phasors form a horizontal line in the vicinity of a resonant point. Further analysis of the I-Q phasors is underway.

## Phase-compensated I and Q Graphs

The post-processing leads to the phase compensated I-Q phasers which can then be used to study the nonlinear effects in the microring resonators. The following measurements show how the I-Q phasors change as the laser power increases.

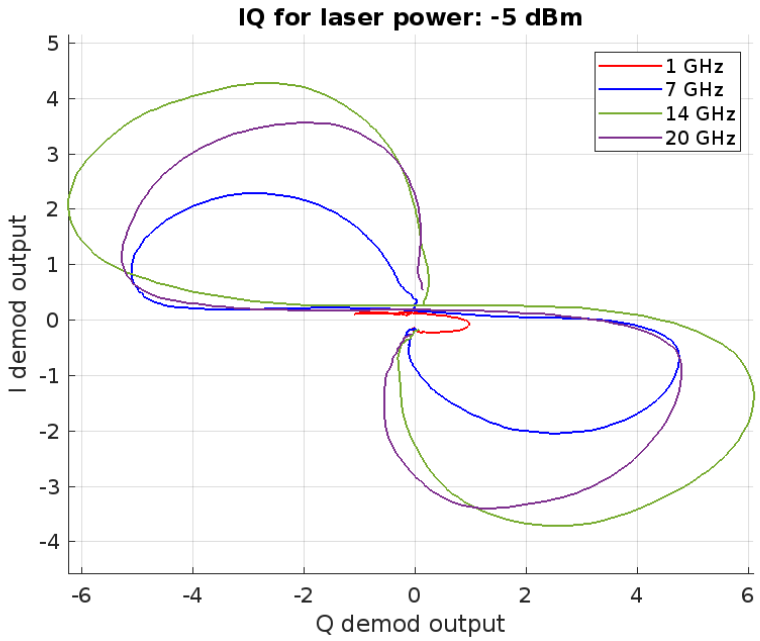


Figure 24. The phase-compensated I-Q phasor for micro-ring resonator in the linear regime (low power).

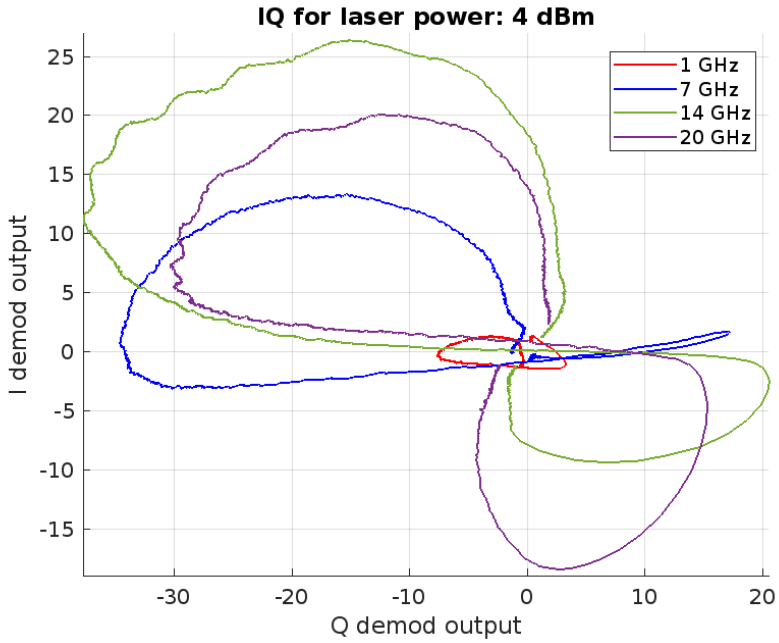


Figure 25. The phase-compensated I-Q phasor for micro-ring resonator in the non-linear regime (high power).

Notice significant deformation of the I-Q phasor lobes as it becomes highly asymmetric. Also the phasor switches the direction of its rotation as the frequency changes from 7 to 14 GHz.

### I and Q Signals as Functions of Modulation Frequency

Thus far we considered the I and Q demodulation signals as functions of the detuning wavelength, i.e. the offset from the resonance. Another set of measurements can be done when the microring resonator is kept at the fixed offset. In this case we can vary the modulation frequency causing the resonant sidebands to move across the width of the resonance. This measurement is inspired by the results presented in [1].

Ideally, one can setup an experiment in which the microring is set close to resonance with the fixed offset. One can then record the I and Q demodulation signals for different modulation frequencies. However, in our approach we took the data from the previous measurements by selecting the values of the I and Q signals corresponding to the same offset of 0.1 nm from resonance. This means that every data point corresponds to a different measurement. The results are shown in Figure 26. Note a significant variation of the data as it was collected from different measurements.

To analyze this dynamics we developed a model for light propagating in a microring resonator which is powered by a single waveguide through evanescent coupling. The model is entirely analytical and has a small number of free parameters.

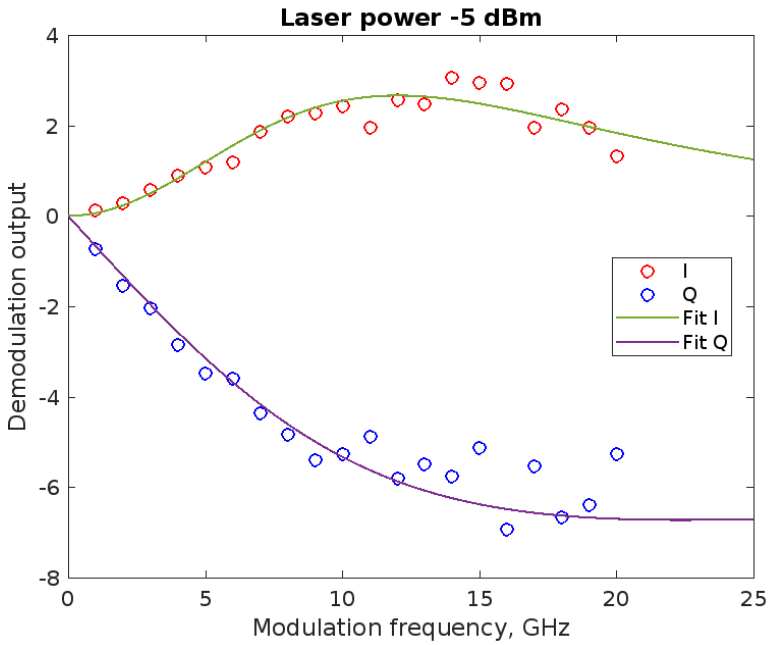


Figure 26. Calculated and measured I and Q demodulation signals.

We used this model to perform the least squares fit of the date shown in Figure 26. In this model we assume linear regime for resonance and high finesse cavity, i.e. the linewidth is much smaller than free spectral range. Analytical function was rotated in I-Q plane in a

way which is similar to the rotation of the I-Q data. When we change the laser wavelength in the vicinity of the resonance, the Q-signal changes linearly while the I-signal has no linear component and changes proportionally to cube of the wavelength detuning. As a result of these fits, we find that the cavity linewidth is 94.8 GHz and the offset from resonance is 45.5 pm (35.4 GHz). Further analysis of these data is currently underway. The research shows that the modulation spectroscopy can be useful for applications of microring resonators in science and technology adding more techniques for their analysis to those already described in literature [5, 6].

## Bibliography


1. "Laser phase and frequency stabilization using an optical resonator," R.W.P. Drever, J. L. Hall, F. V. Kowalski, J. Hough, G.M. Ford, A.J. Munley, and H. Ward, *Applied Physics B,* Vol. 31, no. 2, p. 97 (1983).
2. "Frequency modulation (FM) spectroscopy; Theory of lineshapes and signal-to-noise analysis," G.C. Bjorklund, M.D. Levenson, W. Lenth, and C. Ortiz. *Applied Physics B, Photophysics and laser chemistry,* Vol. 32, no. 3, p. 145 (1983).
3. "Characterization of the LIGO 4-km Fabry–Perot cavities via their high-frequency dynamic responses to length and laser frequency variations," M. Rakhmanov, F. Bondu, O. Debieu and R.L. Savage, *Classical and Quantum Gravity*, Vol. 21, no.5, p. S487 (2004).
4. "High precision optical cavity length and width measurements using double modulation," A. Staley, D. Hoak, A. Effler, K. Izumi, S. Dwyer, K. Kawabe, E. King, M. Rakhmanov, R. Savage, and D. Sigg, *Optics Express,* Vol. 23, p. 19417 (2015).
5. "Optical microresonators: theory, fabrication, and applications," J. Heebner, R. Grover, T. Ibrahim, Springer, 2008
6. "Optical microring resonators: theory, techniques, and applications," V. Van, CRC Press, 2017